

Internal Structure Characterization of Nanoholes and Densely Branched Morphology Thin Films

Darko C*

Department of Materials, University of Manchester, United Kingdom

*Corresponding author: Charles Darko, Department of Materials, University of Manchester, Oxford Road, M13 9PL, Manchester, United Kingdom, Tel: +44 (0)161-306-3568; E-mail: charles.darko@manchester.ac.uk

Received Date: August 07, 2020; Published Date: August 26, 2020

Abstract

The internal structures of thin films, having Nanoholes and densely branched morphologies and prepared from a long chain polystyrene-b-poly (ethylene oxide) (PS-b-PEO) diblock copolymer, were characterized. Using grazing-incidence small- and wide-angle X-ray scattering (GISAXS & GIWAXS), the thickness of the lamellar mesophase repeat unit and the orientation of the PEO crystalline chain stems within the thin film were determined. The dimensions of the internal structures and their orientations were linked to the surface morphologies measured by atomic force microscopy. For the Nanoholes morphology, the film thicknesses were found to deviate from an integer multiple of the diblock copolymer lamellar units (~70 nm) promoting the hole textures. Dewetted architectures were obtained by annealing freshly prepared films under toluene/water vapor environment at an elevated temperature. After that, some PEO chains were able to crystallize within the Dewetted large holes resulting in a densely branched morphology (DBM). The crystalline chain stems of the crystalline lamellar, within the Dewetted large holes, were found to be roughly perpendicular to the film substrate with thicknesses of about 10nm. This is in agreement with the diffusion-limited aggregated model.

Keywords: Nanoholes; Densely Branched Morphology; Diblock Copolymer Thin Films; Crystalline Diblock Copolymer; X-ray scattering

Abbreviations: DBM: Densely Branched Morphology; GISAXS: Grazing-Incidence Small-Angle X-ray Scattering; GIWAXS: Grazing-Incidence Wide-Angle X-ray Scattering; DLA: Diffusion Limited Aggregation; PEO: Poly (Ethylene Oxide); LP: Lorentz and polarization; ODF: Orientational Distribution Function.

Introduction

Fabrication of Nano thin films has been an essential process in the field of Nanotechnology and several Nano templates have been created for many applications [1-5]. Diblock copolymers have been employed in the creation of the thin

film Nano templates because of their unique self-assembly properties [6-11] and they have been applied in the Nano sciences assisting in the fabrication of quantum dots [12,13], Nanowires [14,15], magnetic data storage [16], and bio sensing devices [17]. The self-assembly properties of Diblock copolymers that allow structuring of the thin films into Nano and micro-phase structures (hexagonal, lamellar, gyroid etc.) are controlled by the volume fractions and the Flory-Huggins interaction parameter [18-21] of the polymers involved. The orientation of these Nano and micro-phase structures can be tuned to generate unique surface templates and morphologies that can be controlled by substrate surface treatment [22,23], film thickness [24], the presence of an

external electric field [25], etc.

Nanoholes formation in thin films of diblock copolymers was observed for thin films having a thickness (h) deviating from an integer multiple of the lamellar copolymer period, L [26]. It was noted that Nano templates having whole textured surfaces were formed whenever there is a mismatch between the film thickness and the lamellar period of a symmetric diblock copolymer parallel to the substrate. Such formation of holes requires the interface to deform and stretch (increase area) causing an increase in the surface energy [27]. Also, such formation of holes leads to the relaxation of internal strains that decreases the total energy. Crystallization of polymers is an important topic treated as one of the most practical and experimental problems in polymer science [28]. Polymer crystals are generally not in thermal equilibrium since their formations are hindered by the connectivity of the segments [29]. Consequently, polymer crystals represent metastable states with a significant degree of disorder, mainly characterized by the degree of chain folding. The process of annealing at elevated temperatures, but below the melting temperature (T_m), enhances chain mobility thereby improving the crystalline order. Thus, imperfect crystals are thermodynamically driven towards states of a higher degree of order [30,31].

The crystal formation is a kinetic control process. The processes are; the incorporation of chains where molecules are attached to crystals at the interface between the crystals and melt phases (interface growth kinetics), the molecular diffusion where chains diffuse from the melt phase to the interface and lastly, the diffusion process of latent heat at the interface [32]. Hence, Nano templated patterns such as snowflakes or spherulites, dendrites, seaweed or densely branched morphology (DBM), etc., from crystalline diblock copolymers are considered to be controlled by molecular self-assembly which is cooperative movements of a large number of connected monomers [33-38]. For a crystalline diblock copolymer, the resulting patterns promoted by molecular organizations or reorganizations are affected by the problems of chain folding, lamellar thickening or chain diffusion. The mechanisms can be linked to the diffusion-limited aggregation processes (DLA) [39,40]. The DLA promote the production of a finger-like branched pattern caused by the competition between material transport at the surface of the crystalline finger and the attachment to the crystal in quasi-two-dimensional (2D) geometry.

Crystallization of Poly (ethylene oxide) (PEO) chains have been used to induce different surface patterns because of the PEO chain folding and the diffusion process mechanisms involved [41-44]. It was noted that substrate adsorption effects impose limitations on the chain folding but water assisted the diffusion of the chains (i.e. PEO aggregates under humid

chamber) and enabled chains to diffuse towards the crystal front to form crystalline lamellar [41]. It was explained that the transition from fractal-like patterns to DBM structures was due to the limited availability of polymer chains in the diffusion field and that higher humidity conditions lowered the crystal lamellae growth. Also, Meyer et al. [45] observed the crystallization of PEO chains in Dewetted ultrathin films and obtained highly branched lamellar morphology because of the DLA processes. Besides, Zhai X, et al. [46] observed different patterns like dendrite, seaweed, compact structure, and square single crystals by crystallizing PEO chains at different crystallization temperatures (T_c) in ultrathin films. Under such investigations, it was noted that at a particular set T_c , the chain folding could be explained by the DLA process.

The main question in all the above studies is how the chains are aligned within the thin films. Revealing the chain fold and the mesophase repeat unit orientations within the thin films as well as the quantification of the repeat lamellar units will contribute to the understanding of the complex polymer crystallization processes. This study focuses on the internal thin films characterization of the Nanoholes and densely branched morphology from a long chain poly (styrene-*b*-ethylene oxide) (PS-*b*-PEO) crystalline diblock. The lamellar repeat unit and the crystalline orientations were analyzed and compared to the surface morphologies.

Experimental

The P(S-*b*-PEO) diblock copolymer was purchased from PSS, Mainz. The blocks have molar masses of 109kg/mol each with a polydispersity index of 1.09. The volume fraction for PEO, f_{PEO} , is 0.46 leading to lamellar structure. The melting temperature, T_m , of PEO was found to be 62°C while the glass transition temperature (T_g) of PS is 98°C by Differential Scanning Calorimetry.

For the formation of Nanoholes, three thin films were prepared by spin coating toluene solutions at 20,25 and 30mg/ml concentrations onto UV/ozone cleaned Silicon wafers resulting in film thicknesses of 110, 170 and 220nm, respectively. The film thicknesses were determined by ellipsometry. After spin coating, the films were annealed at T_c of 40°C, for an hour, in a humid atmosphere (i.e. 90% relative humidity) using a heating plate from Instec, USA. The heating plate was placed in a vacuum oven chamber with inner dimensions of 30cm×30cm×40cm. After annealing, the samples were dried overnight by quenching the temperature of the oven, at a rate of 0.5°/min, to room temperature under vacuum with a vacuum pressure of 10-3mbar. The films were later kept at room temperature (i.e. at 20-27°C). It was confirmed that the water vapor did not influence the surface morphology formed (see supplementary data). It may have assisted small internal PEO chain mobility because of the

hygroscopic nature of PEO [41], while the PS chain remains partially glassy. Thus, there was no further microphase separation.

A freshly prepared sample having a film thickness of 170nm was Dewetted by following the same procedure and condition (i.e. 90% relative humidity) above but placed under toluene/water vapor environment. Toluene is a selective solvent for PS [47], but can dissolve both the PS and the PEO, hence used in the preparation of the PS-b-PEO solution before spin coating. The surface morphologies were investigated using an optical microscope with differential interference contrast (Axio Imager from Carl Zeiss, Jena, Germany) and an Axio-Cam video camera. Detailed images of the surface texture were obtained by tapping mode AFM using a JSPM-5200 (Jeol, Echling, Germany) scanning probe microscope with scan rates between 2.8 and 9.3Hz. Silicon cantilevers (NSC35/ABS) having a force constant of 3.5N/m and a resonance frequency of ~135 kHz were used.

To determine the internal lamellar mesophase domain, L , Grazing-Incidence Small-angle X-ray scattering (GISAXS) experiments were performed at beamline BW4, HASYLAB [48]. Sample-to-detector distances were selected between 1.08m and 2m. The wavelength of the X-ray beam was $\lambda=1.388\text{\AA}$ or 1.381\AA . The incident angle, α_i , was varied between 0.15 and 0.5° , thus above the critical angle of the polymer film ($\alpha_{cp} 0.14^\circ$ for $\lambda=1.38\text{\AA}$). The latter is calculated from the X-ray scattering length densities (SLDs) of PS and PEO using the relation $\alpha_{cp} = (\text{SLD}/\pi)^{1/2}$ where λ is the X-ray wavelength [49]. $\alpha_{cp} = 0.135^\circ$ for the amorphous state of PEO in the as-prepared film, which was measured at 1.388\AA , and $\alpha_{cp} = 0.136^\circ$ for the crystalline state of PEO, which was measured at 1.381\AA .

Measurements were carried out at room temperature. Rod-like beam-stops were used to protect the detector from the specular peak and strong diffuse scattering in the plane of incidence. 2D images were given as a function of q_y and q_z , the lateral and the normal components of the scattering vector, respectively. The measuring times were between 8 and 1200s. Parallel lamellar resulted in diffuse Bragg sheets (DBS) along q_z -axis. To analyze their positions as a function of α_i , intensity profiles along q_z were created by integrating over the region $q_y = -0.009$ to $+0.009\text{\AA}^{-1}$. The peaks observed in these intensity profiles along q_z were analyzed using a model for lamellar structures in the distorted wave Born approximation (DWBA) [50]. In this model, the peak positions, q_z , of the DBS were found to depend on L , and the incident angle by:

$$q_z = \frac{2\pi}{\lambda} \left\{ \sin \alpha_i + \sqrt{\sin^2 \alpha_p + \left[\frac{m\lambda}{L} \pm \sqrt{\sin^2 \alpha_i - \sin^2 \alpha_p} \right]^2} \right\} \quad (1)$$

where m denotes the order of reflection. In this way, refraction at the air-polymer interface as well as reflections at the polymer/substrate interface was taken into account.

The orientation of the crystalline PEO chains within the films was also investigated. Grazing-Incidence Wide-angle X-ray scattering (GIWAXS) experiments were performed at Risø National Laboratory, Roskilde, Denmark. A Rigaku rotating anode with λCu , $k\alpha = 1.542\text{\AA}$ was used together with a Fuji film image plate having pixel sizes of $50\mu\text{m} \times 50\mu\text{m}$. The scattering geometry described by Apitz D, et al. [51], with a sample-detector distance of 124mm and a α_i of 0.18° was used for all samples. Measurements were done at room temperature under vacuum, and the images were interpolated to reciprocal space units (q_x, q_z). A region near the q_z axis in reciprocal space is not available when using a fixed incidence angle.

The GIWAXS data were analyzed (including indexing) by comparing them with simulated results using Sim Diffraction software [52-54]. It incorporates the unit cell of PEO that include atomic positions, the geometrical Lorentz and polarization (LP) corrections, and is specifically designed to model samples with varying degree of anisotropy and preferred orientation. The PEO block crystallizes in a monoclinic crystalline lattice defined by the following parameters: $a=8.05\text{\AA}$, $b=13.04\text{\AA}$, $c=19.48\text{\AA}$ and $\beta=125.4^\circ$ [55]. The conformation of PEO is a (7/2) helix which means that seven monomeric units turn two times per fibre period. In the classical uniaxial distribution models (e.g. Kratky O, et al. [56]; Breiby DW, et al. [52,53], the director of a crystallite (in polymers often the chain axis) orients at an angle χ with respect to the sample normal, with an orientation distribution function (ODF), $f(\chi)$. On average, all crystallites orienting with a certain χ assume all possible rotational angles about the director. Note that this model assumes no in-plane orientation of the crystallites, often referred to as "2D powder" or cylindrical symmetry. Thus, in the simulations, the c -axis orientation ("director") of the PEO crystal unit cell with respect to the film normal was varied systematically according to an ODF with a given width, and the crystallites were rotated about the director while maintaining in-plane isotropy [54]. The "rods in soft matrix" model of Kratky O, et al. [56] was found to describe the observed scattering well for the samples with a low degree of preferred orientation. In the Kratky O, et al. [56] model, the crystallites are considered stiff rods in an affine matrix, and when the matrix is stretched by an elongation ratio λ_K , the rods obtain an ODF of,

$$f(\chi) = \frac{1}{4\pi} \frac{\lambda_K^3}{\left[\lambda_K^3 - (\lambda_K^3 - 1) \cos^2 \chi \right]^{3/2}} \quad (2)$$

The simulations were carried out for the settings of the

actual scattering geometry, such as α_i , the λ and the sample to detector distance.

Results and Discussion

Nanoholes

Observations of large and tiny Nanoholes were made on the freshly prepared films but with a very rough texture. The observed Nanoholes within a freshly prepared film were attributed to flow instability within the solvent-rich long PS-*b*-PEO chain films created by the Marangoni instabilities [57] and the fast evaporation of the volatile toluene solvent. Moreover, it was observed that slow evaporation provides enough solvent leveling time that hinders the Marangoni instabilities and promotes smooth surfaces [58]. In this work, the fully extended PEO chain length of molar mass 109,000g/

mol is: $\kappa=luN \sim 689\text{nm}$ (where $lu=0.2783\text{ nm}$ is the monomer length and the degree of polymerization $N=2477$) [55]. The fully extended PS chain length of molar mass 109,000g/mol is: $\kappa=luN \sim 160\text{nm}$ (where $lu=0.154\text{nm}$ is the monomer length and the degree of polymerization, $N=1038$). The long PS and PEO chains might have influenced the Marangoni effect by delaying the solvent leveling.

After annealing the films at $T_c=40^\circ\text{C}$ under water vapor environment, very smooth hole textures were obtained (Figures 1a-1c). The AFM images revealed large rounded Nano-holes ranging from 480.0 ± 10 to $550\pm 10\text{nm}$ and tiny holes of less than $\sim 5\text{nm}$ diameter lengths. The cross-sections of the large Nanoholes (Figures 1d-1f) revealed whole depths of $35\pm 5\text{ nm}$, $56\pm 5\text{nm}$ and $75\pm 5\text{nm}$ for 110, 170 and 220nm thin films, respectively.

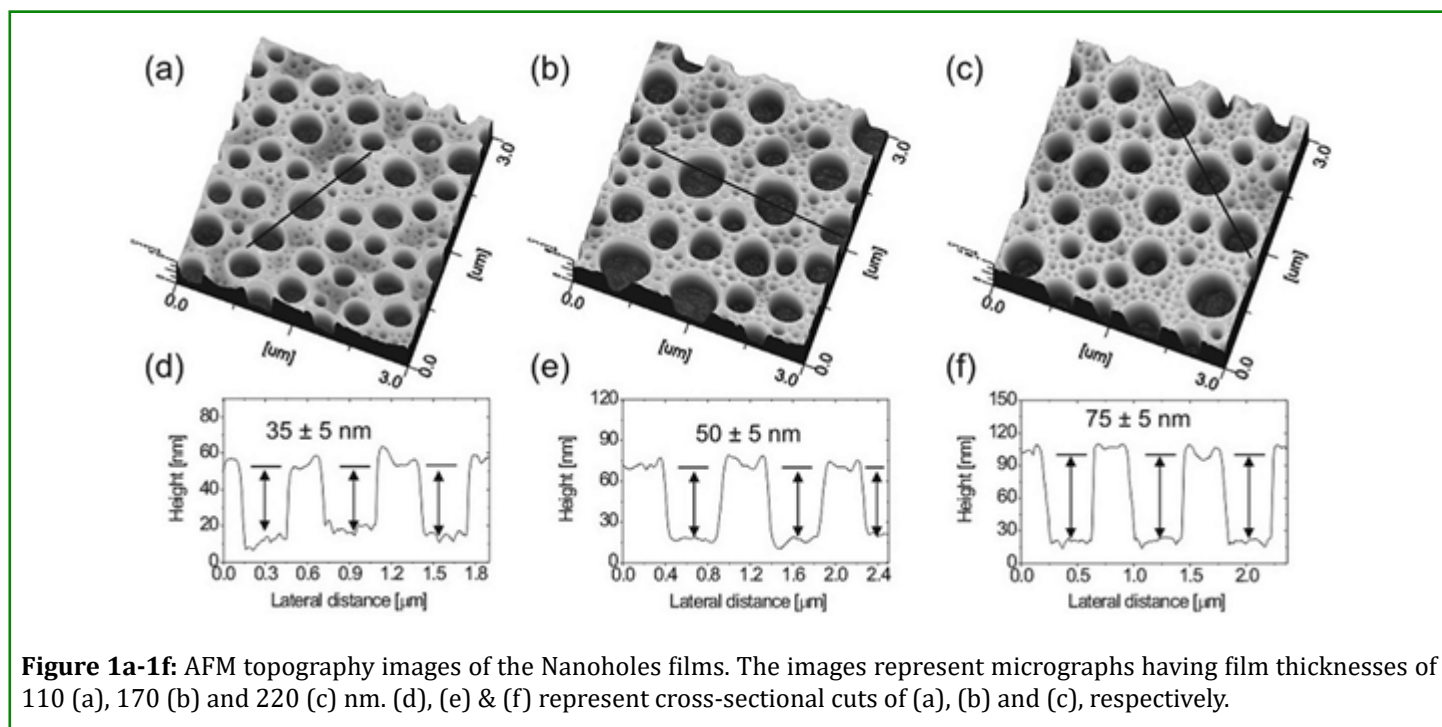
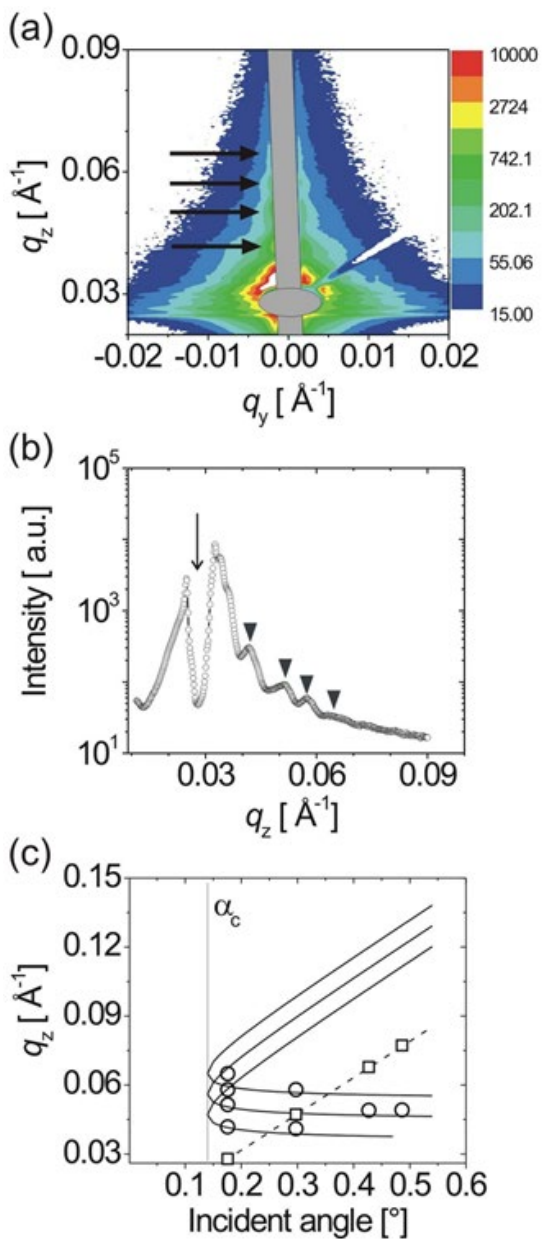


Figure 1a-1f: AFM topography images of the Nanoholes films. The images represent micrographs having film thicknesses of 110 (a), 170 (b) and 220 (c) nm. (d), (e) & (f) represent cross-sectional cuts of (a), (b) and (c), respectively.

The 2D GISAXS image (Figure 2a) enabled the evaluation of the internal diblock copolymer repeat unit, L . It is worth to mention that the films were not annealed above the order-to-disorder transition temperature to properly structure the mesophase repeat layers. Hence, weak DBS resulted from the weak contrast between the crystalline and the amorphous layers (see supplementary GISAXS data). Figure 2a shows weak intensity maxima only along the qz axis; no maxima were observed at finite qy . The peak maxima were indicated by the (black) arrows. The weak intensity maxima were attributed to the DBS's from the crystalline PEO lamellae in the films having their interfaces parallel to the substrate,

separated by amorphous PS layers. Fitting the qz positions of the DBS's (Figure 2b) measured at several incident angles, the repeat distance, L , was determined to be $70\pm 7\text{nm}$ (Figure 2c).

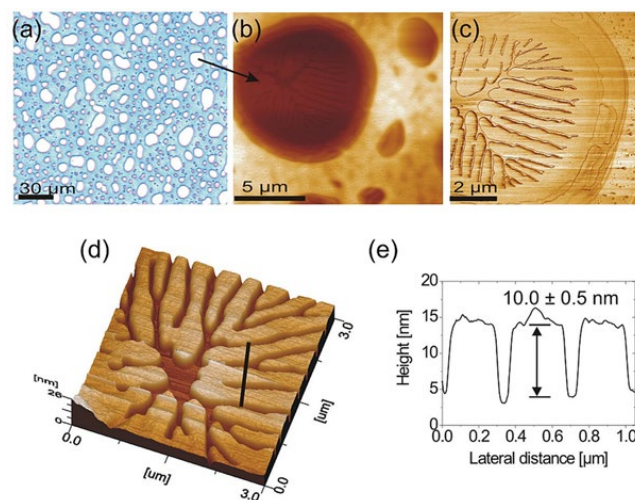
Combining the GISAXS and the AFM results, a distinct relationship between the whole depth and the repeat distances were noted. The lamellar repeat units of $70\pm 7\text{nm}$ can be said to be twice the hole depth (i.e. $35\pm 5\text{nm}$) found on the 110nm film. For the 170nm film, the whole depth of $56\pm 5\text{nm}$ is found to be about 0.8 multiples of L while the 220nm whole depth is close to the repeating units.



Figures 2a-2c: (a): 2D GISAXS image of the 170 nm thin film measured at $\alpha_i = 0.2^\circ$. The grey rectangle and oval shapes indicate the beam stops for the direct beam and the intense secularly reflected peak, respectively. The arrows show the position of the DBS. (b): Intensity profiles along q_z obtained from the 2D image. The area marked \downarrow represents the area of the oval beam stop and the peaks marked \blacktriangledown show the positions of the DBS's. (c): Peak positions q_z from the intensity profiles in (b) as a function of incident angle. Note: Peak positions from images measured at different incident angles were included. Squares: secularly reflected beam, circles: DBS's. Lines: fits of Equation 1. Fitting was made using $L = 70 \pm 7$ nm.

Densely Branched Morphology

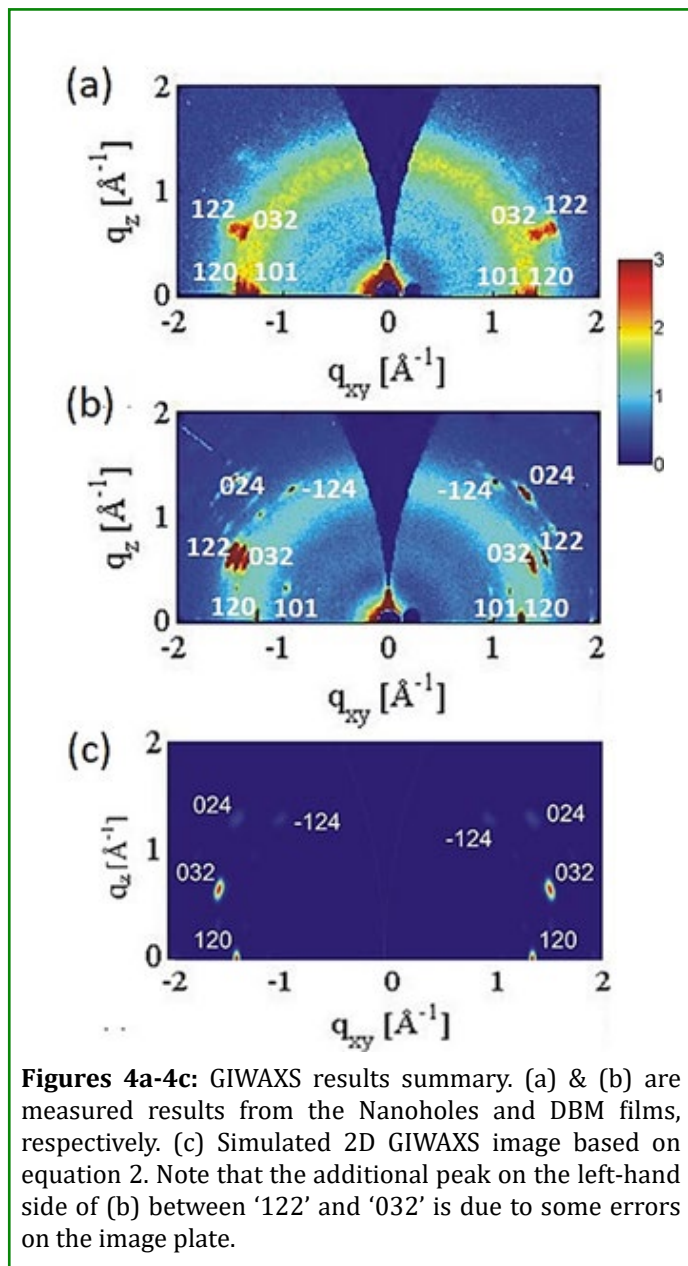
The introduction of toluene/water vapor allowed partial Dewetting of the Nanoholes at the surface of the freshly prepared 170nm film. Quasi-Dewetted large, irregular, micro-sized holes were observed as shown in Figure 3a. It is worth to mention that the Nanoholes were not completely Dewetted and this can be attributed to the mixture of toluene and the water vapor present during the dewetting process. The dewetting process was initiated by the presence of toluene vapor only. As stated earlier, it was suggested that the presence of water vapor assisted the PEO chain mobility during crystallization [41] and might be attributed to the hygroscopic nature of PEO. It is believed that under such conditions, the toluene/water molecules may have diffuse through the PS-PEO film surface into the polymer-silicon interface because of the total equilibrium moisture absorption constant [59], destroying the block copolymer microphase structure at some portions of the film. It is worth to mention that the total equilibrium moisture absorption constant varies with the film thicknesses [59], but this was not the focus of the study.



Figures 3a-3e: Optical and Atomic force micrographs of 170nm film annealed at $T_c = 40^\circ\text{C}$ under toluene/water vapour environment. (a) Optical micrograph of the quasi-Dewetted film. (b) Atomic force micrograph showing DBM within the Dewetted hole, (c) a phase image of (b), (d) detailed atomic force micrograph showing features of the dendritic structures, and (e) cross-sectional graph of the line shown in (d) representing the height of the dendrites.

Thus, there were the crystallization of some free PEO chains and chain folding initiated from the inner whole periphery towards the center resulting in a finger-like DBM (Figures 3b-3d). The DBMs observed have a characteristic finger

height of 10.0 ± 0.5 nm representing the height of the PEO crystal lamellae with an average width (i.e. correlation width) of $\sim 0.3 \mu\text{m}$. The observed DBM is consistent with similar investigations having comparable length scales [60]. In that study, extensive computer simulations based on the DLA were found to agree with the experimental results having the crystalline chain stem orienting perpendicularly to the crystal front (Figure 3e).



In this study, the crystalline orientations within the films were measured to ascertain the chain orientation. The 2D diffraction patterns obtained from the Nanoholes (Figure 4a) and DBM (Figure 4b) films were compared to the simulated

2D image (Figure 4c). The best model was obtained assuming peak width of 0.01 \AA^{-1} , and a Kratky parameter of λK of ~ 0.6 (fwhm = 3°) in the simulations using equation 2. In all, the PEO c-axis was modeled to be perpendicular to the film/substrate interface. However, the Nanoholes film exhibited some isotropic ring intensity distributions that can be attributed to some unoriented chains within the films similar to other research studies [61]. It is believed that during the formation of the Nanoholes, the PEO chains crystallized within the confinement of the rigid PS chains while most of them crystallized in unconfined spaces within the Dewetted large holes during the formation of the DBM's.

Comparing the two experimental patterns with the simulated result, it was clear that both films have the 120, 101, 032 and 122 reflections but the DBM film exhibited additional Bragg reflections of 024 and -124. These additional peaks suggest a larger size of PEO crystals that gives sharper and intense peaks, mostly with perpendicular orientations (Figure 4b). Different simulated orientations can be seen in the supplementary data. The results suggest that the chain stems within the DBM show perpendicular oriented PEO crystal lamellae.

Conclusion

In summary, the lamellar mesophase repeat unit of the diblock copolymer was calculated and the PEO crystalline chain orientations were determined. The dimensions of the internal structures and their orientations were linked to the formed Nanoholes and DBM templates formed. After the films were freshly prepared, and because of the characteristics of the long-chain of the selected PS-PEO diblock, it was noted that several factors contributed to the hole templated Nano textures.

First, it was evaluated that there was a mismatch between the lamellar repeat unit (70 ± 7 nm) and the film thicknesses. Secondly, it was believed that fast evaporation plus flow instability within the solvent-rich long PS-*b*-PEO chain films created by the Marangoni instabilities occurred. Lastly, the mismatch between the lamellar repeat unit and the film thicknesses might have created strong surface tension that influenced the interaction between the block copolymer chains and substrate [62-65]. As observed before (27), under such conditions it requires the interface to deform and stretch (increase area) causing an increase in the surface energy that promoted the hole formation. In this Nanoholes textured films, the PEO chains were not oriented but the hole depths were found to be 0.5L, 0.8L and 1.1L for the 110, 170, 220nm films, respectively.

The large Dewetted hole obtained after the dewetting processes of annealing films under toluene/water vapor

assisted in freeing some of the PEO chains. The free PEO chains were able to crystallize within the quasi-Dewetted holes, with a crystalline lamellae thickness of ~10nm, forming an overall DBM texture. The mechanisms surrounding the formation of the DBM texture is in complete agreement with the DLA model where the crystal chains are said to diffuse and attach perpendicular to the crystal lamellae front. The internal PEO chain stem was analyzed to orient perpendicular the film substrate.

The results contribute to the understanding of crystalline chain folding processes that are complex in nature and also promote the visualization of the resulting morphology. It suggests that the repeat lamellar units and the chain folds within Nano thin films can be linked to the surface architectures.

Acknowledgement

The author will like to thank Prof. Christine Papadakis at the Department of Physics, Technical University Munich, Prof. Guenter Reiter at Albert-Ludwig-University of Freiburg, Prof. Dag W. Breiby at the Norwegian University of Science and Technology and Prof. Jens W. Andreasen, Department of Energy Conversion and Storage, Technical University of Denmark for fruitful discussions and support during the analysis. The author is also very grateful to the Deutsche Forschungsgemeinschaft for financial support (Pa 771/3-1). Part of the work was done at TU München, Garching.

References

1. Michailowski A, AlMawlawi D, Cheng G, Moskovits M (2001) Highly regular anatase nanotubule arrays fabricated in porous anodic templates. *Chemical physics letters* 349(1-2): 1-5.
2. Kim YH, Yoon DK, Jung HT (2009) Recent advances in the fabrication of nanotemplates from supramolecular self-organization. *J Mater Chem* 19(48): 9091-9102.
3. Abdelaal HM (2015) Facile hydrothermal fabrication of Nano-oxide hollow spheres using monosaccharides as sacrificial templates. *Chemistry Open* 4(1): 72-75.
4. Kuila BK, Stamm M (2010) Fabrication of oriented polyaniline Nanostructures using block copolymer Nanotemplates and their optical, electrochemical and electric properties. *J Mater Chem* 20(29): 6086-6094.
5. Gazit E (2007) Use of bio-molecular templates for the fabrication of metal Nanowires. *FEBS J* 274(2): 317-322.
6. Wu H, Higaki Y, Takahara A (2018) Molecular self-assembly of one-dimensional polymer Nanostructures in nanopores of anodic alumina oxide templates. *Progress in Polymer Science* 77: 95-117.
7. Kim JK, Yang SY, Lee Y, Kim Y (2010) Functional nanomaterials based on block copolymer self-assembly. *Progress in Polymer Science* 35(11): 1325-1349.
8. Arsenault AC, Rider DA, Tétreault N, Chen JIL, Coombs N, et al. (2005) Block copolymers under periodic, strong three-dimensional confinement. *J Am Chem Soc* 127(28): 9954-9955.
9. Cushen JD, Bates CM, Rausch EL, Dean LM, Zhou SX, et al. (2012) Thin film self-assembly of poly (trimethylsilylstyrene-*b*-_{D, L}-lactide) with sub-10 nm domains. *Macromolecules* 45(21): 8722-8728.
10. Son JG, Bae WK, Kang H, Nealey PF, Char K (2009) Placement control of Nanomaterial arrays on the surface-reconstructed block copolymer thin films. *ACS Nano* 3(12): 3927-3934.
11. Shi AC, Li B (2013) Self-assembly of diblock copolymers under confinement. *Soft Matter* 9(5): 1398-1413.
12. Kang GB, Kim SI, Kim YT, Park JH (2009) Fabrication of metal Nano dot dry etching mask using block copolymer thin film. *Current Applied Physics* 9(1): S82-S84.
13. Kim J, Hwang GS, Lee DE, Ahn J, Hwang CS, et al. (2019) Directed Self-Assembly of Colloidal Quantum Dots Using Well-Ordered nanoporous Templates for Three-Colored nanopixel Light-Emitting Diodes. *ACS Appl Electron Mater* 1(8): 1626-1632.
14. Liu X, Stamm M (2009) Fabrication of highly ordered polymeric nanodot and Nanowire arrays templated by supramolecular assembly block copolymer nanoporous thin films. *Nanoscale research letters* 4(5): 459-464.
15. Gowd EB, Nandan B, Vyas MK, Bigall NC, Eychmüller A, et al. (2009) Highly ordered palladium Nanodots and Nanowires from switchable block copolymer thin films. *Nanotechnology* 20(41): 415302.
16. Alivisatos AP (1996) Semiconductor clusters, nanocrystals, and quantum dots. *Science* 271(5251): 933-937.
17. Alivisatos P (2004) The use of nanocrystals in biological detection. *Nature biotechnology* 22(1): 47-52.
18. Floudas G, Vazaiou B, Schipper F, Ulrich R, Wiesner U, et al. (2001) Poly (ethylene oxide-*b*-isoprene) diblock copolymer phase diagram. *Macromolecules* 34(9): 2947-2957.
19. Ryu DY, Lee DH, Jeong U, Yun SH, Park S, et al. (2004)

- Closed-Loop Phase Behavior of Polystyrene-*b* lock-poly (*n*-pentyl methacrylate) Copolymers with Various Block Length Ratios. *Macromolecules* 37(10): 3717-3724.
20. Matsen MW, Bates FS (1997) Block copolymer microstructures in the intermediate-segregation regime. *The Journal of chemical physics* 106(6): 2436-2448.
 21. Ryan AJ, Mai SM, Fairclough JPA, Hamley IW, Booth C (2001) Ordered melts of block copolymers of ethylene oxide and 1, 2-butylene oxide. *Physical Chemistry Chemical Physics* 3(15): 2961-2971.
 22. Jin XS, Pang YY, Ji SX (2016) From self-assembled monolayers to chemically patterned brushes: Controlling the orientation of block copolymer domains in films by substrate modification. *Chinese Journal of Polymer Science* 34(6): 659-678.
 23. Park SM, Stoykovich MP, Ruiz R, Zhang Y, Black CT, et al. (2007) Directed assembly of lamellae-forming block copolymers by using chemically and topographically patterned substrates. *Advanced Materials* 19(4): 607-611.
 24. Sepe A, Cernoch P, Stepanek P, Hoppe ET, Papadakis CM (2014) Creation of lateral structures in diblock copolymer thin films during vapour uptake and subsequent drying-Effect of film thickness. *European polymer journal* 50: 87-96.
 25. Morkved TL, Lu M, Urbas AM, Ehrichs EE, Jaeger HM, et al. (1996) Local control of microdomain orientation in diblock copolymer thin films with electric fields. *Science* 273(5277): 931-933.
 26. Lammertink RG, Hempenius MA, Vancso GJ (2000) Morphology and crystallization of thin films of asymmetric organic-organometallic diblock copolymers of isoprene and ferrocenyldimethylsilane. *Langmuir* 16(15): 6245-6252.
 27. Kim YS, Suh KY, Lee HH (1997) Morphology of thin films of lamellar diblock copolymers. *Physical Review E* 56(4): 4887.
 28. Armitstead K, Goldbeck Wood G, Keller A (1992) Polymer crystallization theories. *Advanced in Polymer Science* 100(1): 219-312.
 29. Reiter G, Strobl GR (2007) Progress in understanding of polymer crystallization. Springer 714.
 30. Cheng SZ, Zhang A, Chen J, Heberer DP (1991) Nonintegral and integral folding crystal growth in low-molecular mass poly (ethylene oxide) fractions. I. Isothermal lamellar thickening and thinning. *Journal of Polymer Science Part B Polymer Physics* 29(3): 287-297.
 31. Beekmans LGM, Van der Meer DW, Vancso GJ (2002) Crystal melting and its kinetics on poly (ethylene oxide) by in situ atomic force microscopy. *Polymer* 43(6): 1887-1895.
 32. Hu W (2018) The physics of polymer chain-folding. *Physics Reports* 747: 1-50.
 33. Reiter G, Sommer JU (1998) Crystallization of adsorbed polymer monolayers. *Physical Review Letters* 80(17): 3771.
 34. Goldenfeld N (1987) Theory of spherulitic crystallization. *Journal of crystal growth* 84(4): 601-608.
 35. Utter B, Ragnarsson R, Bodenschatz E (2001) Alternating tip splitting in directional solidification. *Phys Rev Lett* 86(20): 4604-4607.
 36. Brener E, Muller KH, Temkin D (1996) Structure formation and the morphology diagram of possible structures in two-dimensional diffusional growth. *Physical Review E* 54(3): 2714.
 37. Meakin P (1988) Models for colloidal aggregation. *Annual Review of Physical Chemistry* 39(1): 237-267.
 38. Ben JE, Garik P (1990) The formation of patterns in non-equilibrium growth. *Nature* 343: 523-530.
 39. Vicsek T (1984) Pattern formation in diffusion-limited aggregation. *Physical review letters* 53(24): 2281.
 40. Witten TA, Sander LM (1981) Diffusion-limited aggregation, a kinetic critical phenomenon. *Physical review letters* 47(19): 1400.
 41. Wang M, Braun HG, Meyer E (2002) Branched crystalline patterns formed around poly (ethylene oxide) dots in humidity. *Macromolecular rapid communications* 23(14): 853-858.
 42. Wang M, Braun HG, Meyer E (2003) Crystalline structures in ultrathin poly (ethylene oxide)/poly (methyl methacrylate) blend films. *Polymer* 44(17): 5015-5021.
 43. Zhai XM, Wang W, Ma ZP, Wen XJ, Yuan F, et al. (2005) Spontaneous and inductive thickenings of lamellar crystal monolayers of low molecular weight PEO fractions on surface of solid substrates. *Macromolecules* 38(5): 1717-1722.
 44. Zhai X, Zhang G, Ma Z, Tang X, Wang W (2007) Thickening Processes of Lamellar Crystal Monolayers of a Low-Molecular-Weight PEO Fraction on a Solid Surface.

- Macromolecular Chemistry and Physics 208(6): 651-657.
45. Meyer E, Braun HG (2005) Film formation of crystallizable polymers on microheterogeneous surfaces. *Journal of Physics: Condensed Matter* 17(9): 623.
 46. Zhai X, Wang W, Zhang G, He B (2006) Crystal pattern formation and transitions of PEO monolayers on solid substrates from non equilibrium to near equilibrium. *Macromolecules* 39(1): 324-329.
 47. Cong Y, Zhang Z, Fu J, Li J, Han Y (2005) Water-induced morphology evolution of block copolymer micellar thin films. *Polymer* 46(14): 5377-5384.
 48. Roth SV, Dohrmann R, Dommach M, Kuhlmann M, Kroger I, et al. (2006) Small-angle options of the upgraded ultrasmall-angle x-ray scattering beamline BW4 at HASYLAB. *Review of Scientific Instruments* 77(8): 085106.
 49. Tolan M (1999) X-ray scattering from soft-matter thin films-materials science and basic research-introduction. *X-ray scattering from soft-matter thin films* 148: 1.
 50. Busch P, Rauscher M, Smilgies DM, Posselt D, Papadakis CM (2006) Grazing-incidence small-angle X-ray scattering from thin polymer films with lamellar structures-the scattering cross section in the distorted-wave born approximation. *Journal of applied crystallography* 39(3): 433-442.
 51. Apitz D, Bertram RP, Benter N, Hieringer W, Andreasen JW, et al. (2005) Investigation of chromophore-chromophore interaction by electro-optic measurements, linear dichroism, x-ray scattering, and density-functional calculations. *Physical Review* 72(3): 036610.
 52. Breiby DW, Samuelsen EJ (2003) Quantification of preferential orientation in conjugated polymers using X-ray diffraction. *Journal of Polymer Science Part B: Polymer Physics* 41(20): 2375-2393.
 53. Breiby DW, Sato S, Samuelsen EJ, Mizoguchi K (2003) Electron spin resonance studies of anisotropy in semiconducting polymeric films. *Journal of Polymer Science Part B: Polymer Physics* 41(23): 3011-3025.
 54. Breiby DW, Solling TI, Bunk O, Nyberg RB, Norrman K, et al. (2005) Structural surprises in friction-deposited films of poly (tetra fluoro ethylene). *Macromolecules* 38(6): 2383-2390.
 55. Takahashi Y, Tadokoro H (1973) Structural studies of polyethers, $-(CH_2)_mO-$ n. X. Crystal structure of poly (ethylene oxide). *Macromolecules* 6(5): 672-675.
 56. Kratky O (1933) On the deformation mechanism of fibrous materials, I. *Colloid Journal* 64(2): 213-222.
 57. Sultan E, Boudaoud A, Amar MB (2004) Evaporation of a thin film: diffusion of the vapor and Marangoni instabilities. *arXiv* 543: 183-202.
 58. Strawhecker KE, Kumar SK, Douglas JF, Karim A (2001) The critical role of solvent evaporation on the roughness of spin-cast polymer films. *Macromolecules* 34(14): 4669-4672.
 59. Vogt BD, Soles CL, Lee HJ, Lin EK, Wu WL (2005) Moisture absorption into ultrathin hydrophilic polymer films on different substrate surfaces. *Polymer* 46(5): 1635-1642.
 60. Reiter G, Sommer JU (2000) Polymer crystallization in quasi-two dimensions. I. Experimental results. *The Journal of Chemical Physics* 112(9): 4376-4383.
 61. Darko C, Botiz I, Reiter G, Breiby DW, Andreasen JW, et al. (2009) Crystallization in diblock copolymer thin films at different degrees of super cooling. *Physical Review E* 79(4): 041802.
 62. Russell TP, Coulon G, Deline VR, Miller DC (1989) Characteristics of the surface-induced orientation for symmetric diblock PS/PMMA copolymers. *Macromolecules* 22(12): 4600-4606.
 63. Albert JN, Epps TH (2010) Self-assembly of block copolymer thin films. *Materials Today* 13(6): 24-33.
 64. Ma Y, Hu W, Reiter G (2006) Lamellar crystal orientations biased by crystallization kinetics in polymer thin films. *Macromolecules* 39(15): 5159-5164.
 65. Wang Y, Chan CM, Ng KM, Li L (2008) What controls the lamellar orientation at the surface of polymer films during crystallization?. *Macromolecules* 41(7): 2548-2553.